Letters in Applied NanoBioScience
Open-Access Journal (ISSN: 2284-6808)

Article
Volume 15, Issue 1, 2026, 19
https://doi.org/10.33263/LIANBS151.019

Insight into Selective Transfer of Monovalent Metal Ions of Lithium (1+), Sodium (1+), Potassium(1+) via Germanium Carbide Nanocage: A Quantum DFT Modeling

Fatemeh Mollaamin [1,*], Majid Monajjemi [2]

[1] Department of Biomedical Engineering, Faculty of Engineering and Architecture, Kastamonu University, Kastamonu, Turkey
[2] Department of Biology, Faculty of Science, Kastamonu University, Kastamonu, Turkey
* Correspondence: fmollaamin@kastamonu.edu.tr;

Received: 1.09.2025; Accepted: 12.02.2026; Published: 30.03.2026

Abstract: The nanostructures based on Germanium carbide (GeC) are distinctive materials with unique compositional, structural, optical, and electronic properties with exceptional band structure, moderate surface area, and exceptional thermal and chemical stability. Because of these properties, GeC-based nanomaterials have shown promising applications and higher performance in the biological arena. A vast study on ion transport by $GeLi^+C$, $GeNa^+C$, and GeK^+C complexes was probed using computational approaches due to density state analysis of charge density differences (CDD), total density of state (TDOS), and molecular electrostatic potential (ESP) for hybrid clusters of $GeLi^+C$, $GeNa^+C$, and GeK^+C. Functionalizing of Li^+, Na^+, K^+ cations can augment the negative atomic charge of C2, C3, C7–C12, C14, C15, C17, C18, C22–C27, C29, C30 as electron acceptors in $SiLi^+C$, $SiNa^+C$ and SiK^+C nanoclusters. A small portion of Li^+, Na^+, and K^+ entered the Ge–C layer to replace the alkali and alkaline earth metals sites, which could improve the structural stability of the electrode material at high multiplicity. $SiLi^+C$, $SiNa^+C$, SiK^+C nanoclusters have shown the steepest maximums TDOS surrounding –0.30, –0.40, –0.50, and –0.60 a.u. owing to the covalent bond between Li^+, Na^+, K^+ cations and SiC nanostructure with a maximum density of state of ≈ 12. Higher Ge/C content can increase the ion transport capacity of 544.076, 410.370, and 329.181 mAh g^{-1} for $GeLi^+C$, $GeNa^+C$, and GeK^+C nanoclusters for the ion transport process and improve the rate performances by enhancing electrical conductivity. Finally, the unresolved issues, plausible challenges, current status, and future perspectives for the development and design of GeC have been summarized and are expected to promote the medical sectors.

Keywords: germanium carbide nanocage; monovalent ions transport; cell membrane; molecular modeling.

1. Introduction

Nanomaterials are widely applied in photocatalysis, energy, sensing, water purification, biomedicine, and electronics, with further material engineering for future applications. In fact, these are semiconductors in which the pure state of the semiconductor material is deliberately

diluted by adding some quantities of impurities. By so doing, their conductivity and properties are improved relative to those of intrinsic semiconductors [1–3].

Owing to its vast direct bandgap and large exciton binding energy, two-dimensional germanium carbide has already aroused the concern of many scientists [4-6].

Recently, one-dimensional and two-dimensional germanium carbide and tin carbide structures have been predicted and studied only theoretically. The numerical evaluation of the elastic properties, surface Young's and shear moduli, and Poisson's ratio, of GeC and SnC nanosheets and nanotubes, using a nanoscale continuum modelling approach, was investigated. A robust methodology for assessing the elastic constants of GeC and SnC nanotubes without numerical simulation was proposed. The obtained outcomes established a solid basis for future explorations of the mechanical behaviour of 1D and 2D GeC and SnC nanostructures [7].

While prominently represented in the environment, lithium ions are not essential cofactors in biological systems [8]. In contrast, sodium, potassium, calcium, and magnesium are essential cofactors in multiple biological systems, while others, such as iron, zinc, and copper, play roles in specific systems [9,10]. Thus, lithium ions appear to have been isolated from being incorporated as an essential element during the evolution of increasingly complex biological systems [11,12]. Achieving selective transport of monovalent metal ions with high precision and permeability, analogous to biological protein ion channels, has long been explored for fundamental research and various applications, such as ion sieving, mineral extraction, and energy harvesting and conversion. However, it remains a significant challenge to construct artificial nanofluidic devices that balance selective ion transport with high ion permeability [13]. Both Ge and Si anodes received significant attention as next-generation LIB anodes. They share several similarities, including the challenge of a large volume expansion ratio during lithiation, which can lead to capacity fading. However, Ge anodes have several advantages over Si anodes [14].

One material that was widely investigated as a highly promising material for the next generation of anodes in LIBs is germanium (Ge) because of its high specific capacity, superb rate performance, and good cycling reliability due to its fast kinetics for both Li^+ ion diffusion and electronic conduction [15]. However, as with other alloy-based materials used in negative electrodes in LIBs, Ge undergoes large volume changes in the fully lithiated state of $Li_{22}Ge_5$. Numerous strategies have been proposed to overcome this problem, and these strategies are likely to enhance the electrochemical performance of Ge anode materials in LIBs in the near future [16,17].

Currently, the present research aims to explore the possibility of using GeC nanocage for ion transport of Li^+, Na^+, and K^+ by employing first-principles calculations. We have analyzed the structural and electronic properties of $GeLi^+C$, $GeNa^+C$, and GeK^+C nanoclusters using state-of-the-art computational techniques. This work provides the first DFT-based evaluation of germanium carbide nanocluster for Li^+, Na^+, and K^+ coordination and electronic properties. The objectives of this article are to elucidate the intriguing properties associated with the nano-bio-interface of GeC, provide a brief overview of these clusters in advancing nano-biomedicine, and assess their potential as functional components in biomedical applications.

2. Materials and Methods

The aim of this study is to transport alkali metal ions of Li^+, Na^+, and K^+ by GeC nanocages towards the formation of $GeLi^+C$, $GeNa^+C$, and GeK^+C complexes (Figure 1), which can increase the ion transfer in the cell membrane.

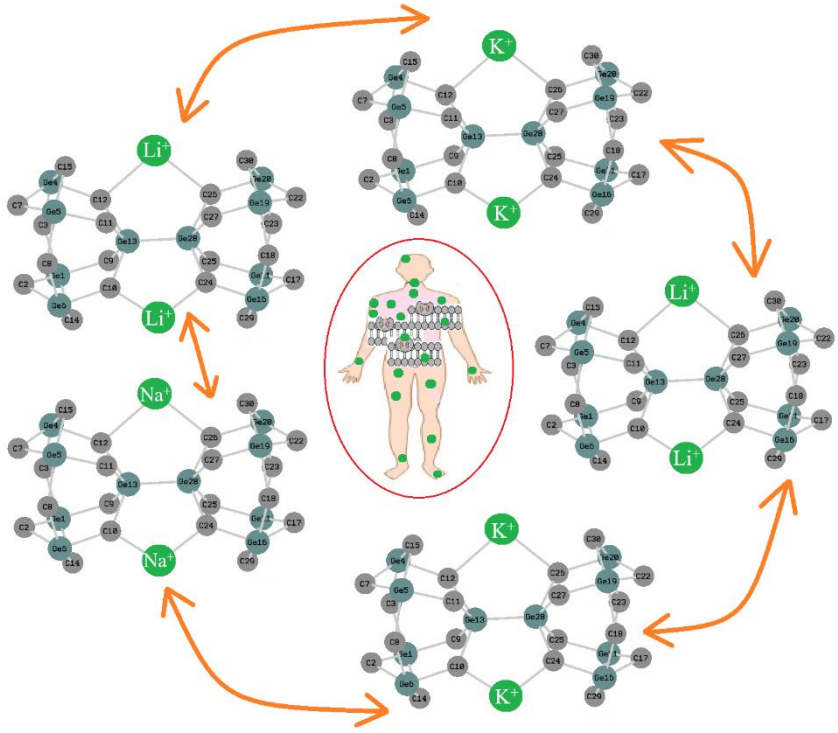

Figure 1. Adding Li^+, Na^+, and K^+ to the GeC nanocluster and formation of **(a)** $GeLi^+C$; **(b)** $GeNa^+C$; **(c)** GeK^+C complexes towards ion transport in biological cells.

All calculations in this paper were performed with the first-principles method based on the density functional theory (DFT) method. The geometries optimization and vibrational frequencies analysis of the models were calculated using DFT with the hybrid exchange-correlation functional B3LYP and 6-311+G(d,p) basis sets [18]. DFT has proven to be an essential tool for exploring the electronic and structural properties of graphene-based electrodes in lithium-ion batteries. While its effectiveness is evident in revealing atomic-level phenomena, current implementations face notable challenges, especially when dealing with complex systems involving defects, interfaces, and lithium diffusion [19].

In this investigation, the computations have been launched by the Coulomb-attenuating method–(Becke, 3-parameter, Lee-Yang-Parr) [CAM–B3LYP–D3] level of theory. This highlights the importance of considering the electronic correlation and dispersion effects in accurately predicting polarizabilities [20].

The analysis of the Bader charge parameter [21] has been illustrated for Ion transport by hybrid clusters of $SiLi^+C$, $SiNa^+C$, and SiK^+C complexes (Figure 1) due to Gaussian 16 revision C.01 computational software [22] and GaussView 6.1 graphical program [23]. The applied basis sets for theoretical calculations of ion transport by $SiLi^+C$, $SiNa^+C$, and SiK^+C complexes have been supported by LANL2DZ and 6–311+G (d,p).

Dispersion forces were considered under the "DFT-D3" method of Grimme with Becke–Johnson damping with multiplicity of +1 and convergence on RMS density matrix=1.00D-08 and convergence on MAX density matrix=1.00D-06 [24,25].

In this investigation, the Onsager model, developed by Frisch, Wong, and Wiberg, has been implemented and utilizes spherical cavities. Even though this implies a less accurate description of the solute-solvent interface, this approximation simplifies the evaluation of energy formation in geometry optimizations and frequency analysis. In fact, a cavity must have a physical sense, as in the Onsager model, and a mathematical ability, as often observed in other descriptions of solvent effects [26]. On the other hand, the cavity must exclude the solvent and define its boundaries as the most probable region of the solute charge distribution [27].

The $Li^+/Na^+/K^+$ insertion might also result in the cleavage of some C–Li^+, C–Na^+, or C–K^+ bonds in the GeC nanocluster and the expansion, providing favorable sites for the subsequent ion insertion in the network (Figure 1). At the same time, the Li^+, Na^+, or K^+ cations could react rapidly with germanium or carbon of GeC nanocluster to form $GeLi^+C$, $GeNa^+C$, and GeK^+C heteroclusters. In addition, the implementation and analysis details of computer DFT modeling have explored possible limitations and pitfalls by means of a number of case studies.

3. Results and Discussion

3.1. Charge density differences analysis.

In Figure 2(a,b,c), charge density differences (CDD) [28] have been shown for $GeLi^+C$, $GeNa^+C$, and GeK^+C nanoclusters with the vibration in the district about –12 to +9 Bohr through co-interaction between alkali metal ions of Li^+31–Li^+32, Na^+31–Na^+32, and K^+31–K^+32. Moreover, the elements of C2, C3, C7–C12, C14, C15, C17, C18, C22–C27, C29, C30 from $GeLi^+C$, $GeNa^+C$, and GeK^+C nanoclusters have displayed the vibration about –12 to +9 Bohr (Figure 2a,b,c).

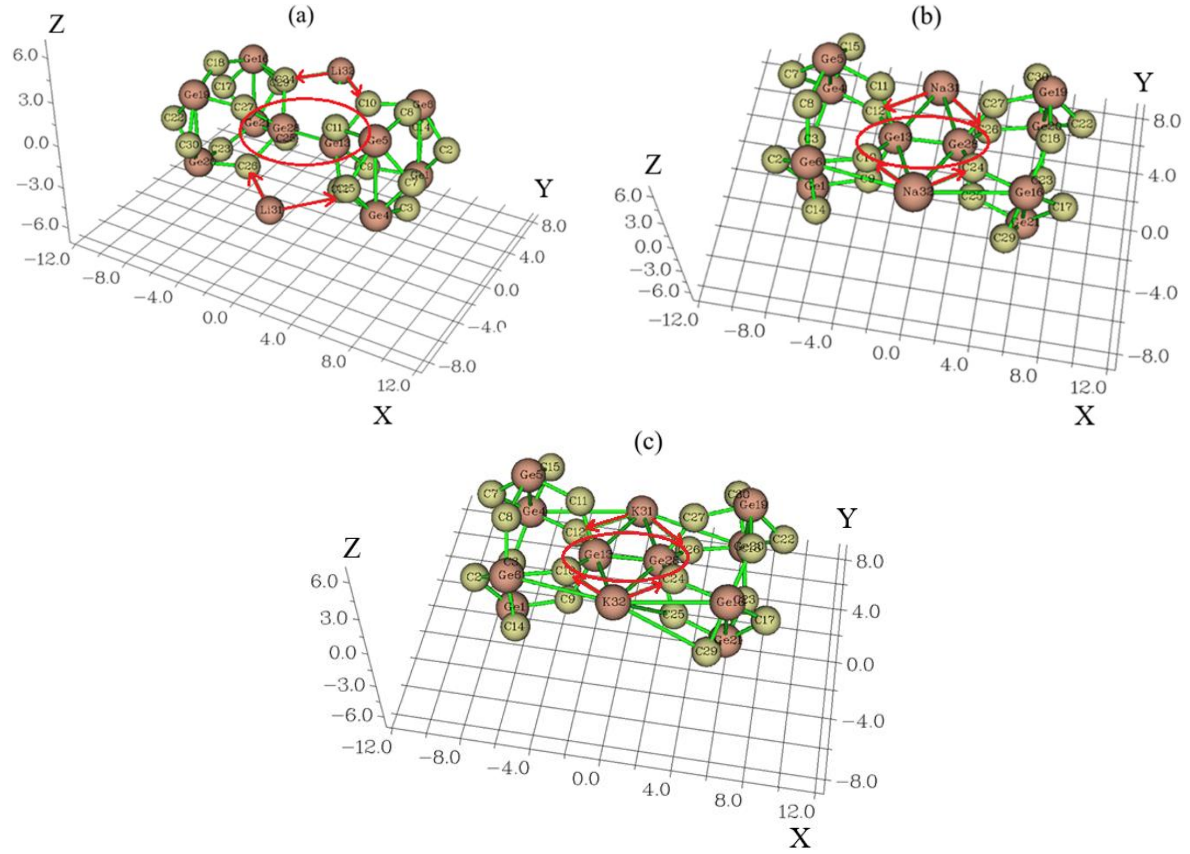

Figure 2. CDD graphs for **(a)** $GeLi^+C$; **(b)** $GeNa^+C$; **(c)** GeK^+C nanoclusters on the X, Y, and Z axes (Bohr).

The charge distribution has been illustrated during alkali metal ions captured by GeC nanostructure towards the formation of $GeLi^+C$, $GeNa^+C$, and GeK^+C nanoclusters, respectively (Table 1).

Table 1. The atomic charge (Q/coulomb) for $GeLi^+C$, $GeNa^+C$ and GeK^+C nanoclusters.

$GeLi^+C$		$GeNa^+C$		GeK^+C	
Atom/Ion	**Q**	**Atom/Ion**	**Q**	**Atom/Ion**	**Q**
C2	–0.310	C2	–0.295	C2	–0.325
C3	–0.170	C3	–0.203	C3	–0.175
C7	–0.274	C7	–0.289	C7	–0.296
C8	–0.185	C8	–0.212	C8	–0.187
C9	–0.320	C9	–0.314	C9	–0.275
C10	–0.705	C10	–0.625	C10	–0.890
C11	–0.302	C11	–0.252	C11	–0.247
C12	–0.856	C12	–0.741	C12	–0.856
C14	–0.263	C14	–0.237	C14	–0.277
C15	–0.255	C15	–0.299	C15	–0.257
Ge16	0.538	Ge16	0.568	Ge16	0.539
C17	–0.308	C17	–0.311	C17	–0.319
C18	–0.172	C18	–0.178	C18	–0.192
C22	–0.277	C22	–0.281	C22	–0.292
C23	–0.169	C23	–0.188	C23	–0.191
C24	–0.704	C24	–0.608	C24	–0.876
C25	–0.270	C25	–0.263	C25	–0.251
C26	–0.759	C26	–0.691	C26	–0.779
C27	–0.456	C27	–0.448	C27	–0.358
C29	–0.286	C29	–0.307	C29	–0.287
C30	–0.257	C30	–0.271	C30	–0.283
Li^+31	0.715	Na^+31	0.661	K^+31	0.897
Li^+32	0.500	Na^+32	0.359	K^+32	0.935

Functionalizing of Li^+, Na^+, K^+ cations can augment the negative atomic charge of C2, C3, C7–C12, C14, C15, C17, C18, C22–C27, C29, C30 as electron acceptors in $GeLi^+C$, $GeNa^+C$ and GeK^+C nanoclusters (Figure 3a,b,c).

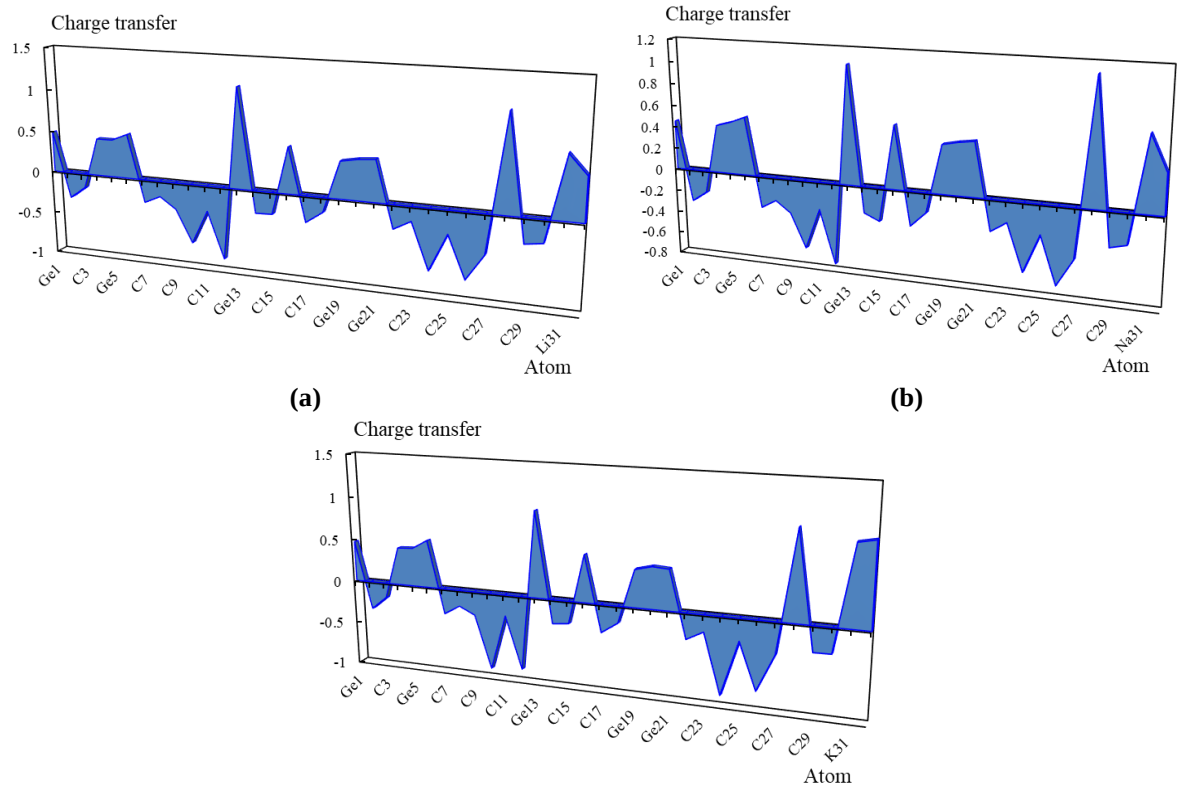

Figure 3. The changes of charge distribution for **(a)** $GeLi^+C$; **(b)** $GeNa^+C$; **(c)** GeK^+C nanoclusters.

Electronic metal–carbon interaction plays a fundamental role in tuning the electrocatalytic behavior of the metal active phase. The basis of the metal–nonmetal interaction is the presence of topological and structural defects, as well as the heteroatom functional group silicon, which breaks the perfect symmetry of a graphene layer, providing preferential nucleation and growth sites for metal nanoparticles and a single metal site. As shown in Figure 2, the electronic states of carbon sites in GeC near the valence band exhibit an electron-acceptor character, whereas metal-ion sites exhibit an electron-donor character.

3.2. Total density of states.

In an isolated system, the energy levels are discrete, and the concept of "density of states (DOS)" is supposed in this situation through the "Multiwfn" program [29,30]. Furthermore, the curve map of "broadened partial DOS (PDOS)" and "overlap DOS (OPDOS)" is valuable for visualizing orbital composition analysis.

Regarding ion transport by $GeLi^{+}C$, $GeNa^{+}C$, and $GeK^{+}C$ nanoclusters, TDOS has been evaluated. This factor can demonstrate the existence of important chemical interactions often on the "convex side" (Figure 4a,b,c).

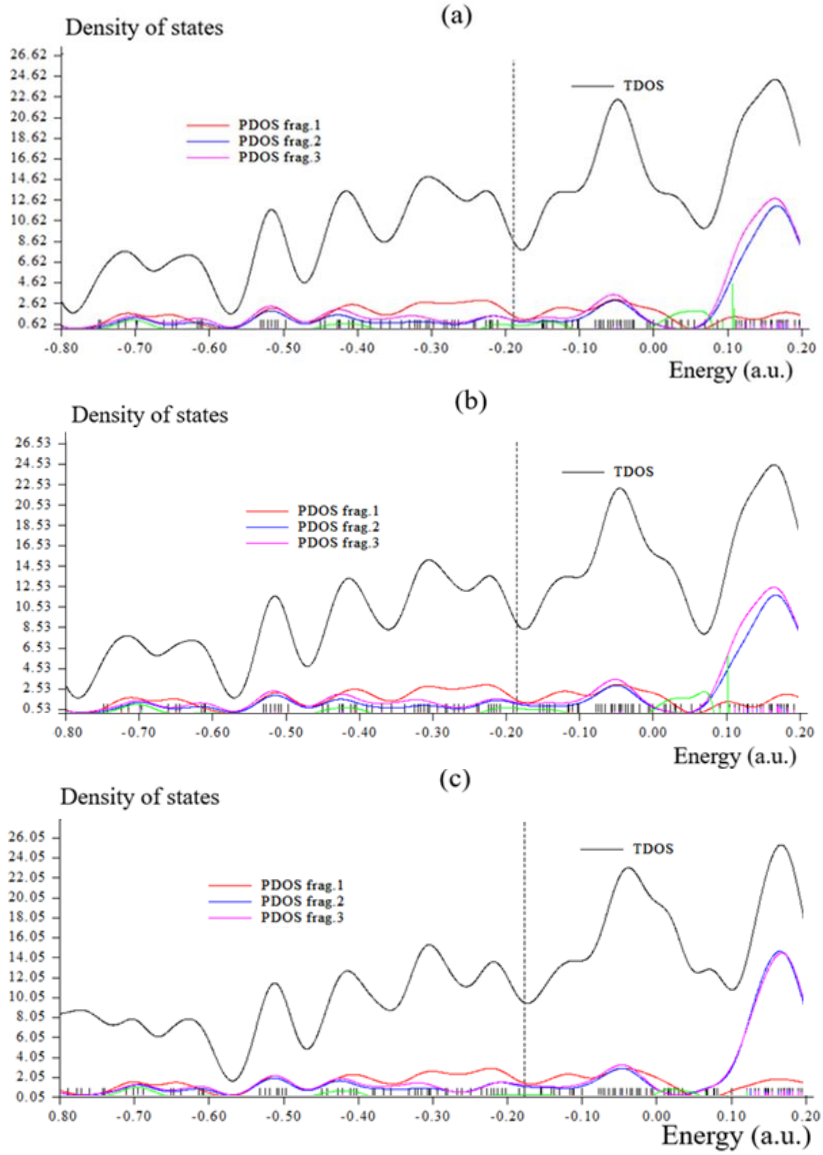

Figure 4. OPDOS/PDOS/TDOS graphs of **(a)** $GeLi^{+}C$; **(b)** $GeNa^{+}C$; **(c)** $GeK^{+}C$ nanoclusters.

$GeLi^+C$, $GeNa^+C$, GeK^+C nanoclusters (Figure 4a,b,c) have shown the steepest maximum TDOS surrounding –0.30, –0.40, –0.50, and –0.60 a.u. owing to the covalent bond between Li^+, Na^+, K^+ cations and GeC nanostructure with a maximum density of state of ≈ 12.

Fragment 1 has been defined for C9 to C12, Ge13, C24 to C27, Ge28, and X31/X32 ($X=Li^+$, Na^+, K^+) in Figure 4 (a,b,c). Fragment 2 has indicated the fluctuation of Ge1, Ge4, and Ge6 beside the similar involved atoms of Fragment 1 in Figure 4 (a,b,c). Finally, it was considered the fluctuation of Ge16, Ge19 to Ge21, C17, C18, C22, C23, C29, C30 in Figure 4 (a,b,c).

An analysis of valence bands and Fermi surfaces in both phases indicates that the density of states crucially depends on the parameter in the Hamiltonian of the system that controls a topological alternation of the Fermi surface. The signature of that alternation is expected to play an important role in quantities closely related to the density of electronic states, such as charge transport and the optical conductivity of the system.

3.3. Molecular electrostatic potential (ESP).

"Molecular electrostatic potential (ESP)" has been commonly used for predicting where nucleophilic and electrophilic reactions might happen for a long time. It is also helpful for understanding hydrogen bonds, halogen bonds, how molecules recognize one another, and how aromatic compounds interact [31]. This function calculates the electrostatic interaction between a single point charge placed at a specific location and the entire system. A positive value means the area is mainly influenced by nuclear charges, while a negative value suggests it's more affected by electronic charges.

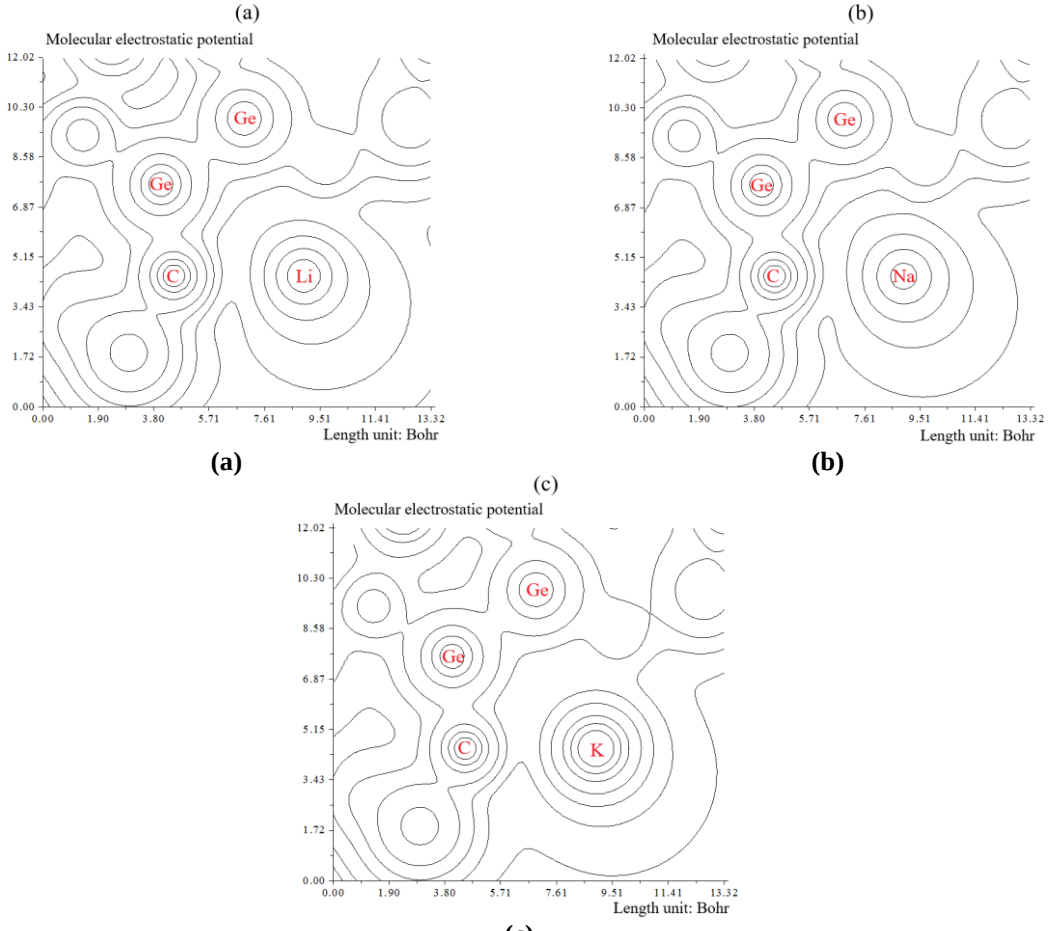

Figure 5. The counter (right side) and shaded (left side) maps of ESP graphs for **(a)** $GeLi^+C$; **(b)** $GeNa^+C$; **(c)** GeK^+C nanoclusters.

Trapping of Li^+, Na^+, and K^+ cations by GeC nanostructure (Figure 5a,b,c) towards the formation of $GeLi^+C$, $GeNa^+C$, and GeK^+C nanoclusters might be described by ESP graphs using Multiwfn due to achieving their delocalization/localization characterizations [32] of electrons and chemical bonds (Figure 5a,b,c).

$GeLi^+C$ (Figure 5a), $GeNa^+C$ (Figure 5b), GeK^+C (Figure 5c) have demonstrated the electron delocalization through an isosurface map with labeling atoms of C10, C12, Ge13, C24, C26, Ge28, X31/X32 ($X=Li^+$, Na^+, K^+). In fact, the counter map of ESP can confirm that $GeLi^+C$, $GeNa^+C$, and GeK^+C nanoclusters may augment the efficiency of ion transport (Figure 5a,b,c).

ESP is meaningful in describing features of these potentials and has been utilized to understand the interactive tendencies of molecules in condensed phases. Therefore, it focuses on surface electrostatic potentials and a variety of statistically derived quantities defined in terms of them.

Besides, the intermolecular orbital overlap integral is important in the illustration of intermolecular charge transfer, which can compute HOMO-HOMO and LUMO-LUMO overlap integrals between Li^+, Na^+, K^+ cations and GeC nanostructure. The layered germanium carbide improved by alkali metal ions of lithium (1+), sodium (1+), and potassium (1+) has indicated the structural stability of Li^+-, Na^+-, and K^+-ion heteroclusters through the reported stability energies in Table 2. Moreover, the intermolecular orbital overlap integral is important in discussions of intermolecular charge transfer, which can calculate HOMO-HOMO and LUMO-LUMO overlap integrals between the alkali metal ions and germanium carbide. The wavefunction level we used was CAM–B3LYP–D3/6–311+G(d,p) that corresponds to HOMO and LUMO, respectively (Table 2). Therefore, E_{LUMO} (a.u.), E_{LUMO} (a.u.), and the local bandgap energies (ΔE/a.u.) and immobile charges induced by polarization discontinuity are simultaneously controlled throughout the structures, and optimized band profiles are eventually achieved for $GeLi^+C$, $GeNa^+C$, and GeK^+C nanoclusters (Table 2). A small portion of Li^+, Na^+, and K^+ entered the Ge–C layer to replace the alkali metal ions sites, which could improve the structural stability of the nanocluster at high multiplicity, thereby improving the capacity rate of 544.076, 410.370, and 329.181 mAh g^{-1} for $GeLi^+C$, $GeNa^+C$, and GeK^+C complexes, respectively (Table 2).

Improving the thermoelectric efficiency of such materials is achieved by simultaneously increasing the electrical conductance across the highest occupied molecular orbital (HOMO)-lowest unoccupied molecular orbital (LUMO) gap.

Table2. Stability energy (kcal/mol), dipole moment (debye), LUMO (eV), HOMO(eV), energy gap (ΔE) (eV), and cell capacity (C, mAh g^{-1}) for $GeLi^+C$, $GeNa^+C$, and GeK^+C nanoclusters.

Heteroclusters	$E_s \times 10^{-3}$ (kcal/mol)	Dipole moment (debye)	E_{HOMO} (eV)	E_{LUMO} (eV)	$\Delta E=E_{LUMO}-E_{HOMO}$ (eV)	C (C, mAh g^{-1})
$GeLi^+C$	–507.966	1.118	–5.157	–4.092	1.064	544.076
$GeNa^+C$	–498.711	1.213	–5.061	–4.215	0.846	410.370
GeK^+C	–533.565	0.864	–4.821	–4.249	0.571	329.181

The charge surfaces produced at the metal spot, which introduce a dipole in the GeC nanocage, can attach to the surface via ion-quadrupole and ion-induced dipole interactions. The consequences show that the GeC nanocage is appropriate for ion adsorption. These investigations could introduce a perspective on modeling new materials using GeC nanocages for ion transfer.

4. Conclusions

Li^+, Na^+, and K^+ metal ions captured by silicon carbide towards the formation of $GeLi^+C$, $GeNa^+C$, and GeK^+C nanoclusters were studied by computational methods. The changes in charge density defined a notable charge transfer in $GeLi^+C$, $GeNa^+C$, and GeK^+C. Due to the semiconducting nature of GeC, it is usually composited with C for better ionic and electronic conductivities. It is well established that enhancing Li^+, Na^+, or K^+ in biological cells can augment the ion transport. Functionalizing of Li^+, Na^+, K^+ cations can augment the negative atomic charge of C2, C3, C7–C12, C14, C15, C17, C18, C22–C27, C29, C30 as electron acceptors in $GeLi^+C$, $GeNa^+C$ and GeK^+C nanoclusters. The results of this research article indicate that the architectural design of $X_2(GeC)$ ($X = Li^+$, Na^+, K^+) can augment the capacity of biological cells. $GeLi^+C$, $GeNa^+C$, GeK^+C nanoclusters have shown the steepest maximums TDOS surrounding –0.30, –0.40, –0.50, and –0.60 a.u. owing to the covalent bond between Li^+, Na^+, K^+ cations and GeC nanostructure with a maximum density of state of ≈ 12. A small portion of Li^+, Na^+, or K^+ entered the Ge–C layer to replace the alkali metal ions sites could improve the structural stability of the electrode material at high multiplicity, thereby improving the capacity retention rate of 544.076, 410.370, and 329.181 mAh g^{-1} for $GeLi^+C$, $GeNa^+C$, and GeK^+C complexes, respectively. This research article covers the state-of-the-art synthetic strategies used to prepare the materials, the basic structure, and a panorama of different optimization strategies that lead to improved physicochemical properties responsible for biological applications. Computational design can be used to establish a surface-state model of the interaction between the GeC nanocage and ion separation in the body, ensuring safety and effectiveness. Therefore, future research should place greater emphasis on theoretical simulations to accurately and in-depth study nanobiointeractions, paving the way for safe and effective biomedical applications of the GeC nanocage bio-interface.

Author Contributions

Conceptualization, F.M.; methodology, F.M.; software, F.M.; validation, F.M. and M.M.; formal analysis, F.M. and M.M.; investigation, F.M. and M.M.; resources, F.M. and M.M.; data curation, F.M.; writing—original draft preparation, F.M.; writing—review and editing, M.M.; visualization, F.M. and M.M.; supervision, F.M.; project administration. The authors have read and agreed to the published version of the manuscript.

Institutional Review Board Statement

Not applicable.

Informed Consent Statement

Not applicable.

Data Availability Statement

Not applicable.

Funding

This research received no funding.

Acknowledgments

In successfully completing this paper and its research, the authors are grateful to Kastamonu University.

Conflict of Interest

The authors declare no conflict of interest.

References

1. Feliczak-Guzik, A. Nanomaterials as Photocatalysts—Synthesis and Their Potential Applications. *Materials* **2023**, *16*, 193, https://doi.org/10.3390/ma16010193.
2. Mollaamin, F.; Monajjemi, M. Graphene-based resistant sensor decorated with Mn, Co, Cu for nitric oxide detection: Langmuir adsorption & DFT method. *Sensor Review* **2023**, *43*, 266-279, https://doi.org/10.1108/SR-03-2023-0040.
3. Khan, H.; Kunchala, R.K.; Ganguli, A.K. Nanomaterials in catalysis: insights from electrocatalysis, photocatalysis and photoelectrocatalysis. *Proc. Indian Natl. Sci. Acad.* **2025**, *91*, 444-468, https://doi.org/10.1007/s43538-024-00349-z.
4. Rahman, M.S.; Islam, M.R.; Sarkar, A.K.; Apurba, I.K.G.G. Tuning the physical properties of monolayer germanium carbide through strain engineering. *J. Comput. Electron.* **2025**, *24*, 79, https://doi.org/10.1007/s10825-025-02317-2.
5. Abdullahi, Y.Z.; Ersan, F. Theoretical design of porous dodecagonal germanium carbide (d-GeC) monolayer. *RSC Adv.* **2023**, *13*, 3290-3294, https://doi.org/10.1039/D2RA07841D.
6. Mollaamin, F. Anchoring of 2D layered materials of $Ge_5Si_5O_{20}$ for (Li/Na/K)-(Rb/Cs) batteries towards Eco-friendly energy storage. *BMC Chem.* **2025**, *19*, 233, https://doi.org/10.1186/s13065-025-01593-0.
7. Fernandes, J.V.; Pereira, A.F.G.; Antunes, J.M.; Chaparro, B.M.; Sakharova, N.A. Numerical Simulation Study of the Mechanical Behaviour of 1D and 2D Germanium Carbide and Tin Carbide Nanostructures. *Materials* **2023**, *16*, 5484, https://doi.org/10.3390/ma16155484.
8. Hart, D.A. Lithium Ions as Modulators of Complex Biological Processes: The Conundrum of Multiple Targets, Responsiveness and Non-Responsiveness, and the Potential to Prevent or Correct Dysregulation of Systems during Aging and in Disease. *Biomolecules* **2024**, *14*, 905, https://doi.org/10.3390/biom14080905.
9. Dobosy, P.; Illés, Á.; Endrédi, A.; Záray, G. Lithium concentration in tap water, bottled mineral water, and Danube River water in Hungary. *Sci. Rep.* **2023**, *13*, 12543, https://doi.org/10.1038/s41598-023-38864-6.
10. De-Paula, V.J.; Forlenza, O.V. Lithium modulates multiple tau kinases with distinct effects in cortical and hippocampal neurons according to concentration ranges. *Naunyn Schmiedebergs Arch. Pharmacol.* **2022**, *395*, 105-113, https://doi.org/10.1007/s00210-021-02171-6.
11. Osete, J.R.; Akkouh, I.A.; Ievglevskyi, O.; Vandenberghe, M.; de Assis, D.R.; Ueland, T.; Kondratskaya, E.; Holen, B.; Szabo, A.; Hughes, T.; Smeland, O.B.; Steen, V.M.; Andreassen, O.A.; Djurovic, S. Transcriptional and functional effects of lithium in bipolar disorder iPSC-derived cortical spheroids. *Mol. Psychiatry* **2023**, *28*, 3033-3043, https://doi.org/10.1038/s41380-023-01944-0.
12. Salem, D.; Fecek, R.J. Role of microtubule actin crosslinking factor 1 (MACF1) in bipolar disorder pathophysiology and potential in lithium therapeutic mechanism. *Transl. Psychiatry* **2023**, *13*, 221, https://doi.org/10.1038/s41398-023-02483-6.
13. Liu, J.; Li, B.; Lu, G.; Wang, G.; Zheng, J.; Huang, l.; Feng, Y.; Xu, S.; Jiang, Y.; Liu, N. Toward Selective Transport of Monovalent Metal Ions with High Permeability Based on Crown Ether-Encapsulated Metal–Organic Framework Sub-Nanochannels. *ACS Appl. Mater. Interfaces* **2024**, *16*, 26634-26642, https://doi.org/10.1021/acsami.4c05672.
14. Gavrilin, I.M.; Kudryashova, Y.O.; Murtazin, M.M.; Tsiniaikin, I.I.; Pavlikov, A.V.; Kulova, T.L.; Skundin, A.M. Electrochemical Synthesis and Application of Ge-Sn-O Nanostructures as Anodes of Lithium-Ion Batteries. *Appl. Nano* **2023**, *4*, 178-190, https://doi.org/10.3390/applnano4020010.
15. Jo, C.; Wen, B.; Jeong, H.; Park, S.K.; Son, Y.; De Volder, M. Spinodal Decomposition Method for Structuring Germanium–Carbon Li-Ion Battery Anodes. *ACS Nano* **2023**, *17*, 8403-8410, https://doi.org/10.1021/acsnano.2c12869.

16. Li, P.; Zhang, H.; Meng, L.; Ding, Y.; Wang, J.; Lou, X.; Bai, H. *In Situ* Synthesis of Germanium Particles Decorated in Conjugated N-doped Carbon Matrix: Boosting the Performance of the Lithium-Ion Battery. *ACS Applied Energy Materials* **2023**, *6*, 362-370, https://doi.org/10.1021/acsaem.2c03259.
17. Sharma, V.; Ghatak, K.; Datta, D. Amorphous germanium as a promising anode material for sodium ion batteries: a first principle study. *J. Mater. Sci.* **2018**, *53*, 14423-14434, https://doi.org/10.1007/s10853-018-2661-1.
18. Mollaamin, F. Competitive Intracellular Hydrogen-Nanocarrier Among Aluminum, Carbon, or Silicon Implantation: a Novel Technology of Eco-Friendly Energy Storage using Research Density Functional Theory. *Russ. J. Phys. Chem. B.* **2024**, *18*, 805–820, https://doi.org/10.1134/S1990793124700131.
19. Mollaamin, F.; Monajjemi, M. Electric and Magnetic Evaluation of Aluminum–Magnesium Nanoalloy Decorated with Germanium Through Heterocyclic Carbenes Adsorption: A Density Functional Theory Study. *Russ. J. Phys. Chem. B* **2023**, *17*, 658-672, https://doi.org/10.1134/S1990793123030223.
20. Adekoya, D.; Qian, S.; Gu, X.; Wen, W.; Li, D.; Ma, J.; Zhang, S. DFT-Guided Design and Fabrication of Carbon-Nitride-Based Materials for Energy Storage Devices: A Review. *Nano-Micro Letters* **2020**, *13*, 13, https://doi.org/10.1007/s40820-020-00522-1.
21. Henkelman, G.; Arnaldsson, A.; Jónsson, H. A fast and robust algorithm for Bader decomposition of charge density. *omput. Mater. Sci.* **2006**, *36*, 354-360, https://doi.org/10.1016/j.commatsci.2005.04.010.
22. Frisch, M.J.; Trucks, G.W.; Schlegel, H.B.; Scuseria, G.E.; Robb, M.A.; Cheeseman, J.R.; Scalmani, G.; Barone, V.; Petersson, G.A.; Nakatsuji, H.; Li, X.; Caricato, M.; Marenich, A.V.; Bloino, J.; Janesko, B.G.; Gomperts, R.; Mennucci, B.; Hratchian, H.P.; Ortiz, J. V.; Izmaylov, A. F.; Sonnenberg, J.L.; Williams-Young, D.; Ding, F.; Lipparini, F.; Egidi, F.; Goings, J.; Peng, B.; Petrone, A.; Henderson, T.; Ranasinghe, D.; Zakrzewski, V.G.; Gao, J.; Rega, N.; Zheng, G.; Liang, W.; Hada, M.; Ehara, M.; Toyota, K.; Fukuda, R.; Hasegawa, J.; Ishida, M.; Nakajima, T.; Honda, Y.; Kitao, O.; Nakai, H.; Vreven, T.; Throssell, K.; Montgomery, J.A., Jr.; Peralta, J.E.; Ogliaro, F.; Bearpark, M.J.; Heyd, J.J.; Brothers, E.N.; Kudin, K.N.; Staroverov, V.N.; Keith, T.A.; Kobayashi, R.; Normand, J.; Raghavachari, K.; Rendell, A.P.; Burant, J.C.; Iyengar, S.S.; Tomasi, J.; Cossi, M.; Millam, J.M.; Klene, M.; Adamo, C.; Cammi, R.; Ochterski, J.W.; Martin, R.L.; Morokuma, K.; Farkas, O.; Foresman, J.B.; Fox, D.J. Gaussian 16, Revision C.01, Gaussian, Inc., Wallingford CT, **2016**.
23. Dennington, R.; Keith Todd, A.; Millam John, M. GaussView, Version 6.06.16. Semichem Inc., Shawnee Mission, KS, USA, **2016**.
24. Kohn, W.; Sham, L.J. Self-Consistent Equations Including Exchange and Correlation Effects. *Phys. Rev.* **1965**, *140*, A1133, https://doi.org/10.1103/PhysRev.140.A1133.
25. Mollaamin, F.; Monajjemi, M. Adsorption ability of Ga_5N_{10} nanomaterial for removing metal ions contamination from drinking water by DFT. *Int. J. Quantum Chem.* **2024**, *124*, e27348, https://doi.org/10.1002/qua.27348.
26. Zhou, J.; Doi, M. Derivation of Two-Fluid Model Based on Onsager Principle. *Entropy* **2022**, *24*, 716, https://doi.org/10.3390/e24050716.
27. Doi, M. Onsager principle in polymer dynamics. *Prog. Polym. Sci.* **2021**, *112*, 101339, https://doi.org/10.1016/j.progpolymsci.2020.101339.
28. Xu, Z.; Qin, C.; Yu, Y.; Jiang, G.; Zhao, L. First-principles study of adsorption, dissociation, and diffusion of hydrogen on α-U (110) surface. *AIP Adv.* **2024**, *14*, 055114, https://doi.org/10.1063/5.0208082.
29. Lu, T.; Chen, F. Multiwfn: A multifunctional wavefunction analyzer. *J. Comput. Chem.* **2012**, *33*, 580-592, https://doi.org/10.1002/jcc.22885.
30. Lu, T. A comprehensive electron wavefunction analysis toolbox for chemists, Multiwfn. *J. Chem. Phys.* **2024**, *161*, 082503, https://doi.org/10.1063/5.0216272.
31. Murray, J.S.; Politzer, P. The electrostatic potential: an overview. *WIREs Comput. Mol. Sci.* **2011**, *1*, 153–163, https://doi.org/10.1002/wcms.19.
32. Matta, C.F.; Ayers, P.W.; Cook, R. The Physics of Electron Localization and Delocalization. In Electron Localization-Delocalization Matrices; Matta, C.F., Ayers, P.W., Cook, R., Eds.; Springer International Publishing: Cham, **2024**; Volume112, pp. 7-20, https://doi.org/10.1007/978-3-031-51434-0_2.

Publisher's Note & Disclaimer